2007

Flow, Flow Shear, And Related Profiles In Helicon Plasmas

E. Scime

R. Hardin

C. Biloiu

A. M. Keesee

X. Sun

Flow, flow shear, and related profiles in helicon plasmas

E. Scime, R. Hardin, C. Biloiu, A. M. Keesee, and X. Sun
Department of Physics, West Virginia University, Morgantown, West Virginia 26506-6315

(Received 5 January 2007; accepted 22 February 2007; published online 30 April 2007)

Measurements of the three-dimensional ion flow field and the ion temperature in a cross section of a cylindrical, argon, helicon plasma are presented. When these measurements are combined with radially resolved measurements of the plasma density, electron temperature, neutral density, and neutral temperature, the radial profiles of the ion viscosity and ion-neutral momentum transfer rate can be calculated. The ion viscosity and ion-neutral momentum transfer rate profiles are important input parameters for theoretical models of azimuthal flows arising from the nonlinear interaction of drift waves in helicon sources. The experimentally determined magnitudes and radial profiles reported in this work are significantly different than those used in recent theoretical studies. Measurements of the radial flow of argon neutrals and helium neutrals are also presented for a helicon plasma. © *2007 American Institute of Physics*. [DOI: 10.1063/1.2716687]

I. INTRODUCTION

In a recent report concerning shear flow driven by turbulent fluctuations in a cylindrical plasma device,[1] the authors noted that a lack of measurements of the spatial profile of ion temperature, neutral temperature, and neutral density resulted in significant levels of uncertainty in their determination of the spatial profile of the ion-neutral momentum transfer rate and the ion-ion viscosity—which were required for comparison of their flow measurements to predictions of average azimuthal flow driven by drift-turbulence in a helicon plasma source. In this work, we will present spatially resolved (in two dimensions) measurements of ion temperature, the three-dimensional ion flow velocity, ion density, neutral density, and neutral temperature for argon plasmas in a cylindrical plasma device that can be combined to provide direct measurements of the ion-neutral momentum transfer rate and ion-ion viscosity spatial profiles for helicon plasma sources.

Creation and control of plasma flow and its associated shear is a subject of intense research activity in both the basic plasma physics and fusion plasma communities. Although much of the recent emphasis in the basic plasma physics community has been on instabilities that are more easily excited, or only exist, in the presence of flow shear,[2–5] the fusion plasma community has been more concerned with the suppression of transport[6] or resistive wall modes[7] resulting from the presence of flow shear and bulk rotation, respectively. Holland *et al.*[1,8] reported experimental evidence for zonal flow generation by drift-wave turbulence in a helicon plasma source, measured the Reynolds stress with a four-tip electrostatic probe, and then used their measurements to solve the time-averaged component of the azimuthal ion momentum equation for the magnitude of the time-averaged azimuthal ion velocity. The predicted time-averaged azimuthal ion velocity was generally consistent with measurements of the mean azimuthal plasma velocity based on time delay estimation methods. Solving the ion momentum equation for the time-averaged azimuthal ion velocity required knowledge of the radial profile of the ion-neutral collision frequency and the ion viscosity.

Holland *et al.* argued that the calculated time-averaged azimuthal ion velocity was relatively insensitive to the ion-neutral collision frequency profile and therefore assumed a uniform ion-neutral collision profile. However, although they determined that the calculated time-averaged azimuthal ion velocity obtained from the solution of the ion momentum equation was quite sensitive to the ion viscosity, in their analysis they also assumed that the ion-ion viscosity was spatially uniform (implicitly assuming a centrally peaked ion temperature) in the center of their plasma and decreased stepwise in the outer half of the discharge (we note that measurements in helicon sources demonstrating ion temperature profiles flat or peaked at the edge have been reported previously[9,10]). Other key measurements on which their analysis relied included the magnitude of the ion temperature ($\sim$0.6 eV), generally consistent with previous measurements of ion temperature in helicon sources,[11] and the magnitude of the neutral temperature ($\sim$0.5 eV), an order of magnitude larger than previously reported values for argon helicon plasmas.[12]

In the remainder of this paper, we will first describe the experimental apparatus used to perform the flow and temperature measurements; we will review the measured spatial profiles of flow, temperature, and density; and will then discuss the measurements in terms of ion viscosity and ion-neutral collisionality spatial profiles. Radially resolved measurements of radial neutral flow and neutral temperature in helium plasmas are also presented as they are qualitatively consistent with the argon plasma measurements and confirm that the neutral temperature in helicon sources is only slightly higher than room temperature.

II. EXPERIMENTAL APPARATUS

The measurements described in this work were performed in the HELIX helicon source.[13] The HELIX vacuum chamber (Fig. 1) consists of a 61 cm long Pyrex tube 10 cm in diameter connected to a 91 cm long, 15 cm diameter stainless steel chamber. The chamber has one set of four 6 in.

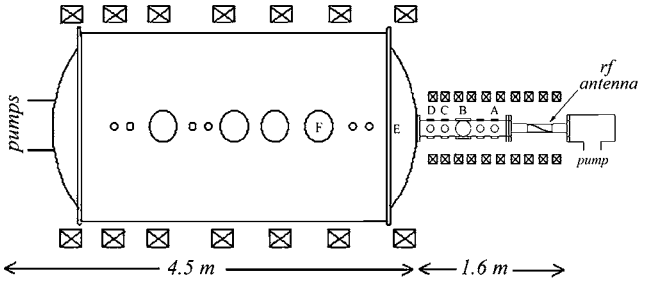

FIG. 1. The HELIX-LEIA system. The 19 cm helical antenna is wrapped around the outside of the Pyrex section of the HELIX chamber between $z=27$ and 46 cm from the right end of the source. Langmuir probe measurements were made position C ($z=126$ cm) in HELIX. 2D LIF measurements were accomplished at position B.

Conflat™ crossing ports in the center of the chamber and two sets of four 2-3/4 in. Conflat™ crossing ports on either side that are used for laser-induced fluorescence (LIF) and spectroscopy diagnostic access. The stainless steel chamber opens into a 2 m diameter space chamber, the Large Experiment on Instabilities and Anisotropies (LEIA). The opposite end of the Pyrex tube is attached to a glass tee. Ten electromagnets produce a steady state axial magnetic field of 0–1400 G in the source. Because of the magnetic field geometry, at both ends of the source the field lines exit the chamber at grounded, conducting boundaries. A mass flow controller is used to introduce gas into the vacuum chamber at the glass tee. Neutral pressures are measured by a Balzers PKR250 full range pressure gauge located in the glass tee and by a Baratron pressure gauge located 35 cm downstream of the antenna. Plasmas are created at neutral pressures ranging from 0.1 to 100 mTorr. Rf power of up to 2.0 kW over a frequency range of 6–18 MHz is coupled into a 19 cm half-wave, right-handed helix antenna to create the steady state plasma. Characteristic electron temperature and densities in HELIX are $T_e \approx 4$ eV and $n \approx 1 \times 10^{13}$ cm^3 as measured with an rf compensated Langmuir probe located 50 cm downstream of the antenna.

The ion and neutral flow velocities, ion and neutral temperatures, and metastable state densities were measured with laser-induced fluorescence[14–18] in a plane perpendicular to the axis of the source. In this work, a collimated laser beam and overlapping focused collection optics are mechanically scanned across the measurement plane. The injection direction of the laser is varied through all three Cartesian directions to obtain the full three-dimensional flow speed in the measurement plane.[19] We note that the measurements reported here are not the first two-dimensional implementation of LIF. Other groups have implemented planar LIF by dispersing the laser beam into a sheet beam through a cross section of the plasma and then capturing two-dimensional (2D) images of the LIF intensity and one-dimensional particle flow along the path of the sheet beam[20,21] Measurement of two ion velocity components at a single spatial location has also been reported previously using a multiplexed LIF apparatus.[22] These LIF measurements go beyond previous work by providing measurements of the three-dimensional ion flow field in a two-dimensional plane, thereby allowing us to determine the radial diffusion of the ions as well as the bulk flow and flow shear in the measurement plane.

A typical LIF measurement consists of sweeping the frequency of a very narrow bandwidth laser through a collection of ions or atoms that have a thermally broadened velocity distribution function (vdf). The illuminated ions or atoms absorb a photon and are pumped into an excited state when the laser appears at the appropriate frequency in their respective rest frames. Measurement of the intensity of the photon emission from the excited state as a function of laser frequency characterizes a typical LIF measurement. For Ar II vdf measurements, our ring dye laser-based LIF laser system (see Ref. 11 for a description of the laser system) is tuned to 611.662 nm (vacuum wavelength) to pump the Ar II $3d^2G_{9/2}$ metastable state to the $4p^2F_{7/2}$ state, which then decays to the $4s^2D_{5/2}$ state by emitting 460.96 nm photons.[23] For He I vdf measurements, the dye laser is tuned to 587.725 nm to pump electrons in the $2p^3P_1^o$ state to the $3d^3D_2$ state. Collisions of the excited state atom with electrons result in a transfer of the excited state electron to the $3p^3P_2^0$ state, which then decays to the $2s^3S_1$ state by emission at 388.975 nm.

For Ar I vdf measurements, our tunable diode laser system (see Ref. 12 for a complete description) is tuned to 667.913 nm to pump the $4s(^2P^o_{3/2})_1$ state to the $4p'(^2P^o_{1/2})_0$ state ($1s_4$ to $2p_1$ in Paschen notation), which then decays to the $4s'(^2P^o_{1/2})_1$ state ($1s_2$) emitting a photon at 750.593 nm. While the $4s(^2P^o_{3/2})_1$ state is not a ground or metastable state, there is a sufficient population for LIF due to direct excitation from the ground state and electron-impact excitation transfer from nearby metastable states $4s(^2P^o_{3/2})_2$ and $4s'(^2P^o_{1/2})_0$ ($1s_5$ and $1s_3$, respectively). For Ar I, jj-coupling must be used to describe the sublevels because the interaction between the spin of each electron and its own orbit is greater than the spin-spin and orbit-orbit interactions.[24]

For both laser systems, the beam is split and 90% is mechanically chopped at ~2 kHz. Dye laser light is coupled into a multimode, non-polarization-preserving fiber optic cable for transport from the laser laboratory to the helicon source, while the diode laser light is injected directly into the helicon source. As the laser frequency is swept over the typical 10 GHz range, the fluorescent emission from the pumped excited state is collected and transported via a fiber optic cable to a filtered (1 nm bandwidth around the fluorescence wavelength), narrowband, high-gain, Hamamatsu photomultiplier tube (PMT). Since the PMT signal is composed of background spectral radiation, electron-impact-induced fluorescence radiation, and electronic noise, a Stanford Research SR830 lock-in amplifier is used to eliminate signals not correlated with the laser modulation. Lock-in amplification is essential since electron-impact-induced emission is several orders of magnitude larger than the fluorescence signal. The signal-to-noise for the measurements reported here ranges from as large as 100:1 to as little as 2:1. The remaining 10% of the beam is passed through an iodine cell for a consistent zero-velocity reference as well as compensation for possible laser drift.[12] Fluorescence from the iodine cell is detected with a photodiode and recorded for each laser frequency.

The LIF collection and injection optics (described in detail in Ref. 19 and shown in Fig. 2) for perpendicular (to the

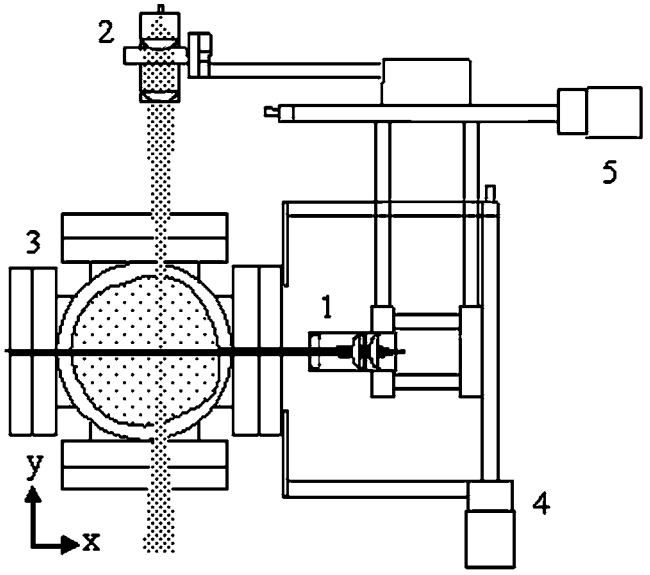

FIG. 2. The 2D scanning apparatus: 1. Beam reducing and polarizing injection optics. 2. Optimized collection optics. 3. Plasma source chamber. 4. *Y* axis scanning stage. 5. *X* axis scanning stage.

magnetic field) measurements are mounted on two independent, but coupled, computer controlled, Velmex™ stepping motor stages, located as shown in Fig. 1. The collimated dye laser injection beam has a diameter of 0.5 ± 0.05 cm across the entire plasma column. The diode laser beam has a diameter of 0.2 ± 0.05 cm across the entire plasma column and is injected without using the motorized injection optics stage. The incident diode laser beam is aligned with the motorized collection optics stage so that scans along the beam can be performed. When the LIF interrogation volume ($\sim 3.9\times10^{-3}$ cm^3) is scanned in the vertical direction, both the injection and collection optics move as a single unit, thereby providing a fixed sample volume as the x component of ion velocity; i.e., $V_{ix}(x_o,y)$, is measured as a function of y position. $V_{ix}(x_o,y)$ is determined by measuring the frequency shift of the measured ion velocity distribution function (ivdf) relative to the natural frequency of the absorption line. Statistical uncertainty in the fits of the ivdf and iodine cell measurement limits the precision of the velocity measurement to ±10 m/s. During collection optics scans, the distance between the collection optics and injection beam remains fixed and the collection spot is scanned along the collimated laser beam, thereby providing a measurement of $V_{ix}(x,y_o)$ and $n(x,y_o)$. For the measurements presented here, the typical spatial coverage of the LIF system was ±3.5 cm in the x and y directions.

A linear polarizer in the injection optics reduces the injected dye laser intensity by a factor of 2. However, by only pumping the π transitions ($\Delta m=0$) in the Ar II $3d^2G_{9/2}$ to $4p^2F_{7/2}$ transition sequence, the much larger Zeeman splitting of the σ transitions ($\Delta m=\pm1$) lines is avoided and the ivdf can be fit with a single thermally broadened Gaussian function. The diode laser polarization axis is aligned with the source magnetic field so that the same principle is employed during diode laser LIF measurements for Ar I. The internal Zeeman splitting of the π lines, Stark broadening, the natural linewidth of the absorption line, and the laser linewidth are ignorable. Velocity distribution function width measurements, i.e., temperature measurements, obtained over the full range of available laser power indicate that power broadening due to saturation of the absorption line[25] is ignorable for the measurements reported here.

Measurements of $V_{iy}(x,y)$ for Ar II and He I are obtained by simply exchanging the injection and collection optical fibers on the 2D scanning apparatus. Because the collection optics do not include a linear polarizer, all the Zeeman split line clusters will contribute to the LIF signal and extraction of the y component of the ion temperature requires a complete deconvolution analysis. However, the bulk flow speed is still easily determined from the frequency shift in the measured vdf. In addition to measurements of $V_{ix}(x,y)$ and $V_{iy}(x,y)$, measurements of $V_{iz}(x,y)$ for Ar II are obtained by injecting the dye laser, after conversion to a single circular polarization, through a window at the right end of the source as shown in Fig. 1. Using a single lens, the parallel optics produce a 0.8 cm diameter, collimated beam at the focal point of the collection optics mounted on the 2D scanning apparatus; yielding a sample volume of $\sim6.3\times10^{-3}$ cm^3. The parallel injection optics are attached to an optical mount that can be manually scanned along the y direction. The entire parallel assembly rests on another computer controlled Velmex™ stage that scans along the x direction. Thus, the parallel ivdf (and therefore the parallel ion flow) can be determined throughout the x,y plane for which the perpendicular flow measurements were obtained. Since the positioning errors for stepping motors are much smaller than the injection and collection spot sizes, the spatial resolution of the flow field measurements is limited by the sizes of the perpendicular and parallel sample volumes.

III. FLOW, TEMPERATURE, AND DENSITY MEASUREMENTS

Using the methods described above, the two-dimensional ion flow velocity field $[V_{ix}(x,y), V_{iy}(x,y)]$ for a cross section of an argon plasma was obtained for four different source configurations: strong magnetic field and low neutral pressure [Figs. 3(a) and 3(b)]; strong magnetic field and high neutral pressure [Figs. 3(c) and 3(d)]; weak magnetic field and low neutral pressure [Figs. 4(a) and 4(b)]; and weak magnetic field and high neutral pressure [Figs. 4(c) and 4(d)]. Each figure shows the total flow velocity field overlaid with a color contour plot of the LIF signal amplitude. In all four cases, the plasma column rotates azimuthally without any application of externally imposed radial electric fields. The largest rotation rates occur at the largest magnetic field strengths and the lowest neutral pressures. For the strong magnetic field with low neutral pressure case [Figs. 3(a) and 3(b)], the tangential velocity at the edge of the discharge peaks at approximately 1500 m/s. Somewhat surprising is the strong azimuthal rotation for the weak magnetic field with low neutral pressure discharge [Figs. 4(a) and 4(b)], which was not in the helicon mode and therefore has a strongly asymmetric LIF intensity profile. The slowest tangential velocities were obtained in the high pressure, weak

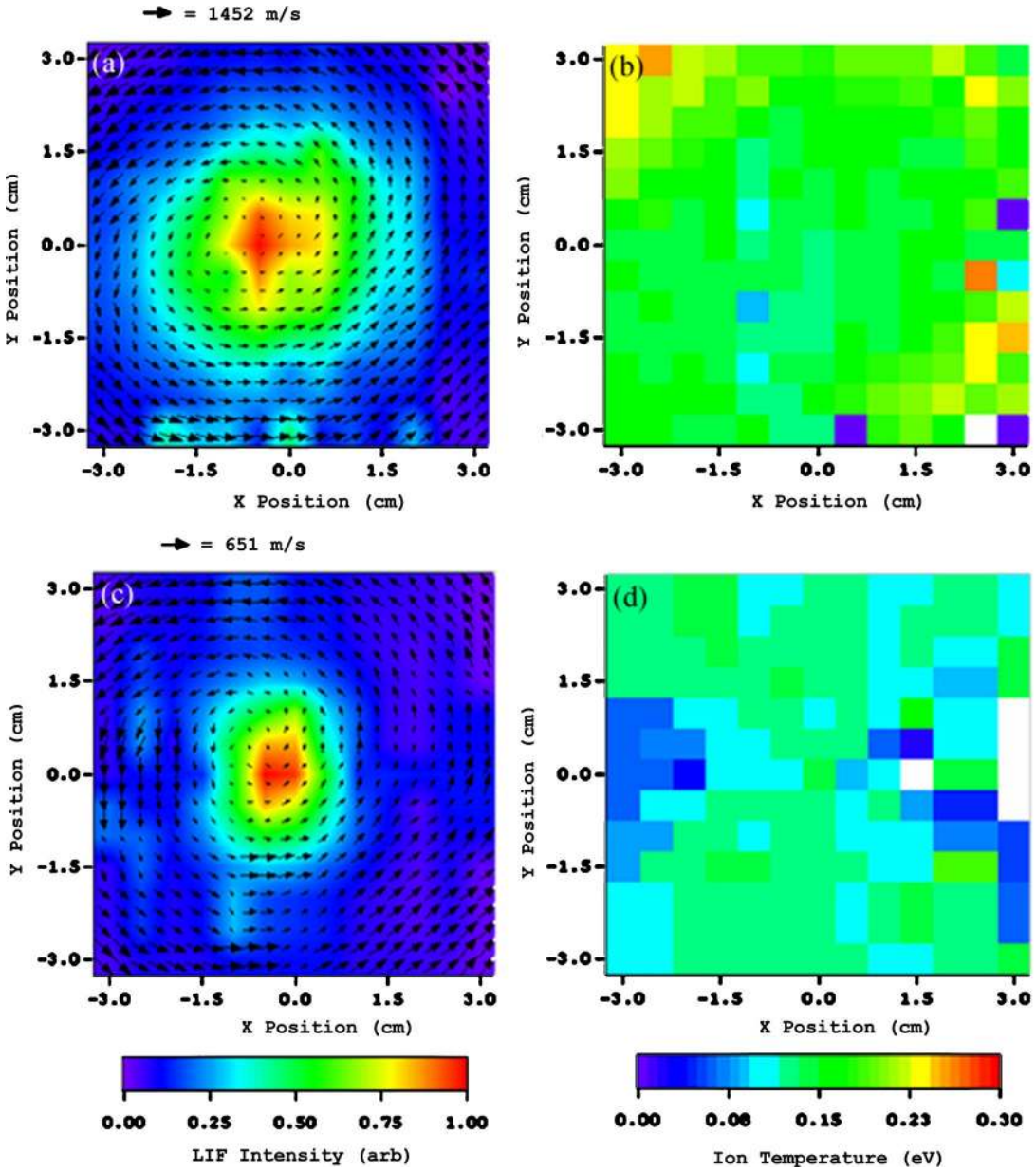

FIG. 3. (Color online) For a radio frequency of $f=9.5$ MHz, $P=3.6$ mTorr, $B_{\mathrm{HELIX}}=716$ G, $B_{\mathrm{LEIA}}=35$ G, and power=750 W, the (a) ion flow velocity field across the plasma column (arrows with scaling given by arrow legend above the plot) overlaid with a normalized contour plot of LIF intensity and (b) the perpendicular ion temperature for the same plasma cross section. For $P=10.1$ mTorr, the (c) ion flow velocity field across the plasma column overlaid with a normalized contour plot of LIF intensity, and (d) the perpendicular ion temperature.

magnetic field case. The ion flow is in the ion diamagnetic direction in all four cases.

In all four cases, there is no evidence of a centrally peaked ion temperature profile in the perpendicular ion temperature measurements. For the strong magnetic field with low neutral pressure case, most similar to the conditions of the Holland *et al.* work,[1] the nominal 0.2 eV ion temperature is largest at the edge of the discharge and decreases towards the center of the discharge. These measurements are consistent with our previous one-dimensional profile measurements that indicated typically flat ion temperature profiles in low to moderate magnetic field strength helicon sources. As the edge lower hybrid frequency approaches the rf driving frequency, a result of changing to a strong magnetic field (i.e., the strong magnetic field cases shown in Fig. 3), the perpendicular ion temperature becomes largest towards the edge of the discharge.[9]

In three of the four cases, the rotation axis of the discharge is located at the slightly off-center peak in the LIF intensity. Recently we demonstrated that the total Ar II LIF signal in a helicon discharge is proportional to the square of the plasma density times the square root of the electron temperature and can therefore be used as a noninvasive, qualitative, measure of the density profile in argon helicon plasmas.[18] Although the relationship between the total LIF signal and ion density is complex, if the metastable ions interrogated via LIF are created by electron impact excitation of ground state ions, the LIF signal intensity should be roughly proportional to the square of the plasma density; i.e.,[26]

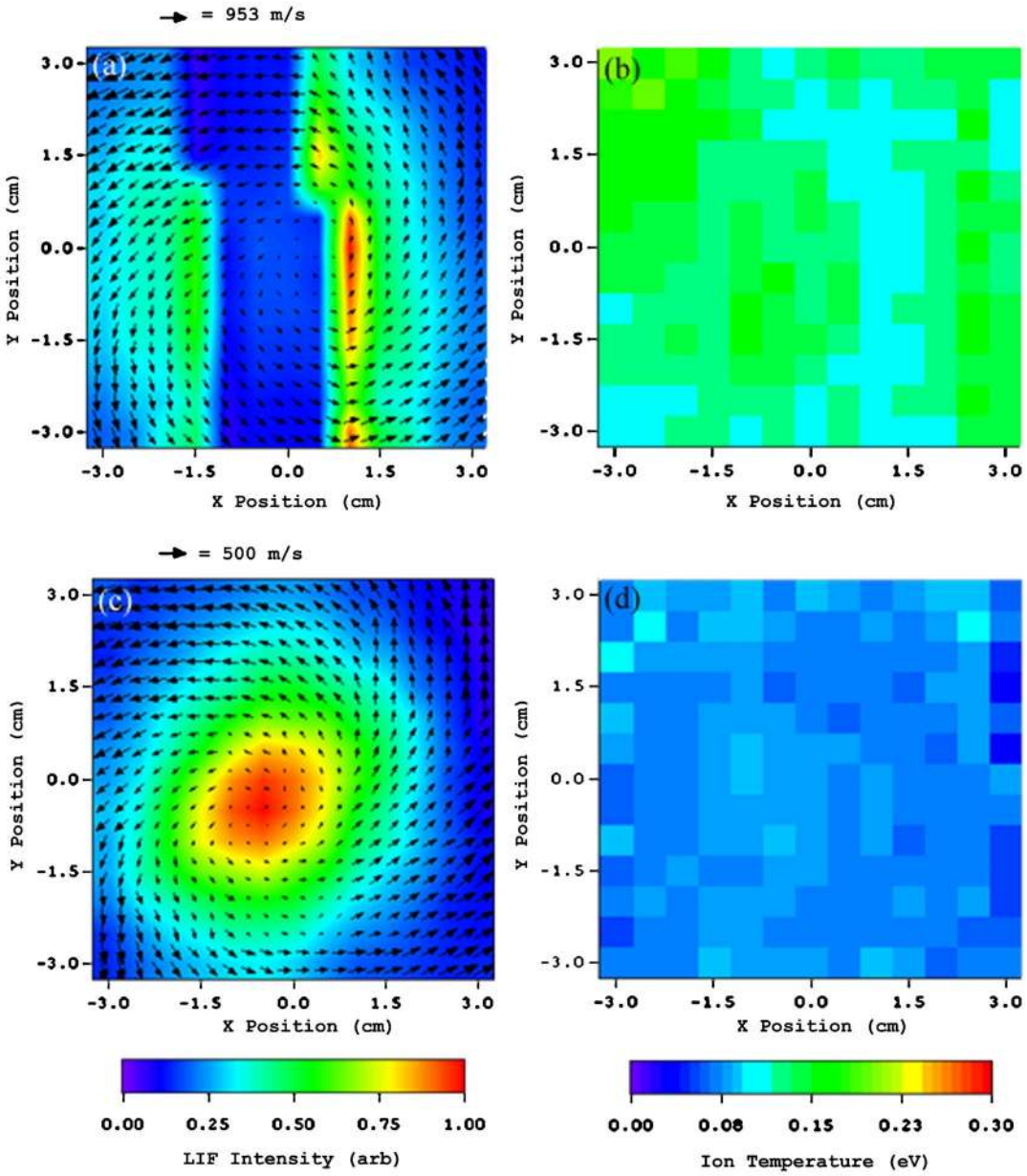

FIG. 4. (Color online) For a radio frequency of $f=9.5$ MHz, $P=3.6$ mTorr, $B_{\mathrm{HELIX}}=436$ G, $B_{\mathrm{LEIA}}=35$ G, and power=750 W, the (a) ion flow velocity field across the plasma column (arrows with scaling given by arrow legend above the plot) overlaid with a normalized contour plot of LIF intensity and (b) the perpendicular ion temperature for the same plasma cross section. For $P=10.1$ mTorr, the (c) ion flow velocity field across the plasma column overlaid with a normalized contour plot of LIF intensity, and (d) the perpendicular ion temperature.

$$n^2 = n_i n_e \approx \frac{n_j}{\langle \sigma v \rangle_{0j} \sum_{i<j} A_{ij}}, \tag{1}$$

where n is the plasma density, n_i the ion density, n_e the electron density, n_j the density of ions in the metastable state, j, probed with the laser (proportional to the total LIF signal), $\langle \sigma v \rangle_{0j}$ is the velocity distribution averaged cross section for electron impact excitation from the ion ground state into state j, and $\Sigma_{i<j} A_{ij}$ is the sum of the spontaneous transition rates from the metastable state to all lower states. The assumption that transitions from other states, including cascades from upper states and excitation from lower metastable states, are not significant source of the interrogated metastable ions is equivalent to claiming that the ion state populations in argon helicon plasmas can be calculated with a steady state coronal model.[27] In support of this assertion, the LIF intensity in the helicon source as a function of rf driving frequency and radial position is compared to the square of the Langmuir probe measured plasma density times the square root of the electron temperature [as suggested by Eq. (1)] in Figs. 5(a) and 5(b), respectively. The comparison in Fig. 5(b) is limited to $r>-2$ cm because insertion of the Langmuir probe beyond $r=-2$ cm (the probe is inserted from the positive radius side of the figure) substantially perturbed the discharge; LIF data were available out to $r=\pm 3.5$ cm. Given that the trends in the LIF and Langmuir probe measurements shown in Fig. 5 are essentially identical, it is reasonable to assume that the peaks in the LIF intensity shown

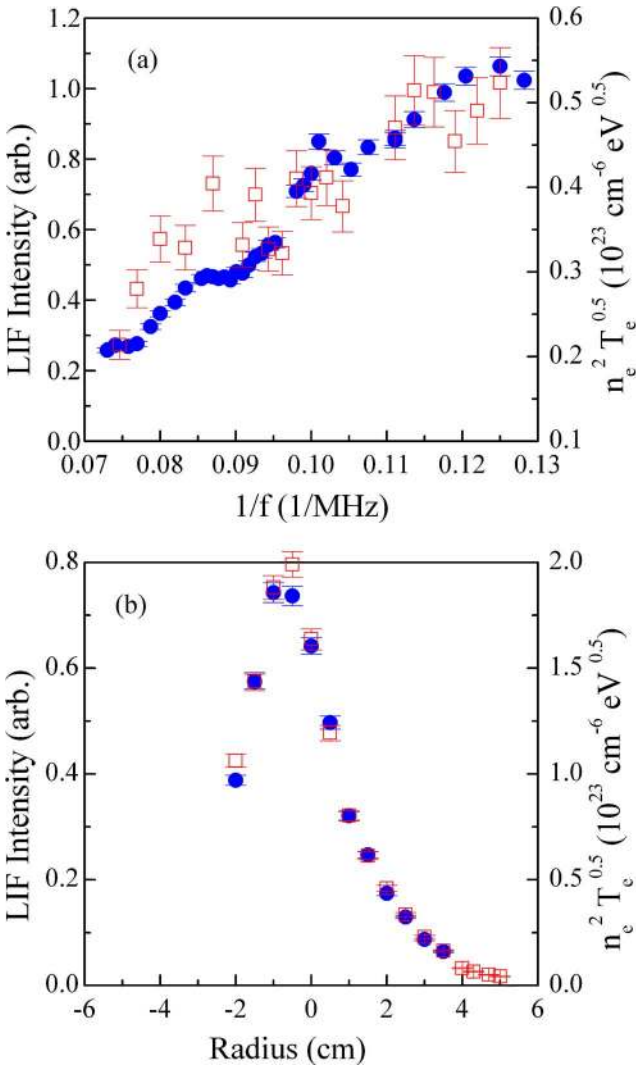

FIG. 5. (Color online) For a rf power of 750 W, B_H=730 G, and B_L =34 G, the LIF intensity (solid circles) and the square of the plasma density times the square root of the electron temperature (open squares) (a) vs rf driving frequency and (b) vs radial position in HELIX. The frequency scan was performed at a neutral pressure of 1.2 mTorr and the radial scan at a neutral pressure of 1.8 mTorr.

in Figs. 3, 4(c), and 4(d) correspond to the peaks in the ground state ion density. In the non-helicon mode case (weak field and low neutral pressure) shown in Figs. 4(a) and 4(b), the rotation axis is located in the middle of what appears to be a hollow LIF intensity profile. For the low pressure plasma conditions of Figs. 4(a) and 4(b), it appears that the LIF signal is dominated by transitions from excited states and not from the ground state.

Measurements of the individual component velocities in the two-dimensional plane also yield important insight into the ion dynamics in a helicon discharge. Shown in Fig. 6(a) are measurements of just the V_x ion velocity. If the plasma were to rotate as a circularly symmetric rigid body, increasing radial distance would yield a linearly increasing tangential velocity ($V_\theta = \omega r$). V_x measurements performed at locations other than the x=0 cm axis would yield values based on a projection of the plasma rotation along the x axis. A simple calculation shows that the combination of rigid body rotation and projection along the laser line of sight (the x axis) should result in V_x measurements that are constant for a fixed y distance from the center of the discharge; i.e., the curves of constant V_x velocity in Fig. 6(a) should look like a series of stacked horizontal bands. Instead, there is a substantial tilt to the contours of constant V_x velocity. The tilt of V_x contours results from an additional radial ion velocity component; which is evident in the measurements of V_x versus radius extracted from Fig. 6(a) for y=0 and shown in Fig. 6(b). Although there is a modest horizontal offset of the peak density in Fig. 8(a), there is no vertical offset and therefore the measurements shown in Fig. 6(b) are a direct measurement of the radial ion flow in the helicon discharge. At the edge of the discharge, the ions have a roughly 400 m/s net outward radial flow. At the location of the maximum in LIF intensity ($x \sim -1$ cm), the radial ion flow is zero—consistent with expectations for the center of a cylindrically symmetric discharge.

As a function of magnetic field strength, vertical slices of the horizontal component of ion velocity are shown in Fig. 7 versus y position; i.e., radius. The three measurements shown in Fig. 7(a) for 424, 587, and 668 G are consistent with rigid body rotation of the plasma column. The rotation frequency increases with increasing magnetic field strength. For the magnetic field strength cases shown in Fig. 7(b), the rotation frequency decreases for the strongest magnetic fields and there is a clear departure from rigid body rotation for radii greater than 2 cm. Thus, for the strongest magnetic fields investigated, the plasma spontaneously rotates and shear in the azimuthal flow spontaneously develops. Such a sheared azimuthal flow profile is roughly consistent with the time-delay measurements of flow shear reported in the strongly magnetized Holland *et al.* plasma source study.[1] Note that around the periphery of the plasma for the strong magnetic field and high pressure case, shown in Fig. 4(c), there are regions of purely vertical and purely horizontal flows; apparently detached from the bulk rotation of the inner portion of the plasma column.

Previous studies by other groups have suggested that strong magnetic fields result in large-amplitude instabilities that increase particle transport and decrease plasma density in helicon sources.[28] The Holland *et al.*[1] study suggested that for similar plasma conditions, nonlinear interactions between collisional drift waves also drive sheared plasma flow. The measured plasma density and azimuthal rotation frequency in HELIX are shown in Fig. 8 as a function of magnetic field strength. At the largest magnetic field strengths, the plasma density and plasma rotation frequency both decrease (and azimuthal flow shear appears). What these measurements cannot ascertain is if the sheared flow arises from nonlinear wave-wave interactions or if the sheared flow itself drives transport-increasing instabilities such as the Kelvin-Helmholtz instability—and thereby reduces the plasma density at large magnetic field strengths.

The full three-dimensional flow field across a plasma cross section is shown in Fig. 9 for a neutral pressure of 3.8 mTorr and a source magnetic field of 652 G. The most remarkable aspect of the parallel component of the ion velocity is that it is largest at the periphery of the discharge.

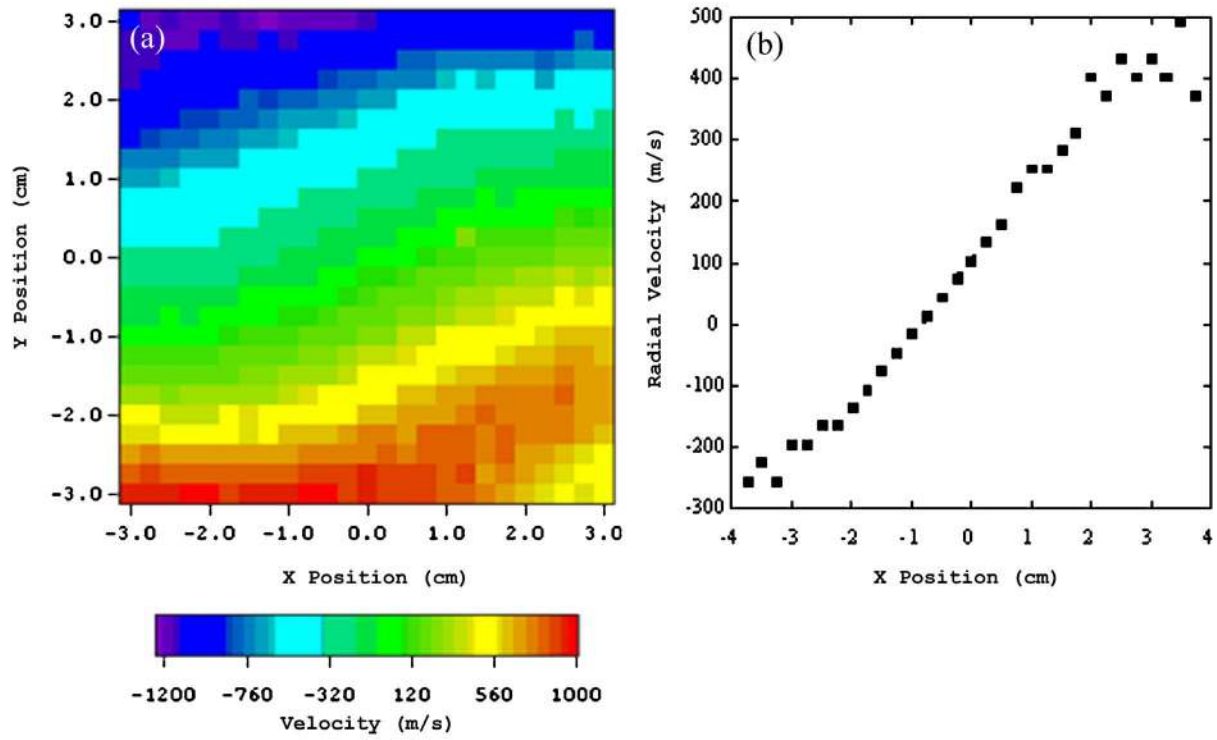

FIG. 6. (Color online) For a radio frequency of $f=9.5$ MHz, $P=3.8$ mTorr, $B_{\mathrm{HELIX}}=652$ G, $B_{\mathrm{LEIA}}=35$ G, and power=750 W, the (a) horizontal component of the ion flow velocity across the plasma column and (b) the horizontal component of the velocity at $y=0$; i.e., the radial ion flow speed.

The magnitude of the parallel ion flow ranges from ~100 m/s along the azimuthal rotation axis to ~300 m/s at $r=3$ cm. For a neutral density profile that is uniform or hollow, it would seem reasonable to expect the parallel velocity to be either spatially uniform or perhaps smallest at the edge where larger neutral densities and therefore more frequent charge exchange collisions would result in increased drag on the ions. However, parallel flow measurements for a range of plasma conditions all indicated that the largest parallel ion flows were at the edge of the discharge.[29] Therefore, both azimuthal and parallel flow shear ($dV_z/dr \neq 0$) appear to be intrinsic properties of helicon sources with an "open-end" geometry.

In helium helicon plasmas, there is little evidence of momentum coupling between ions and neutrals; i.e., across a plasma cross section there is no evidence of an organized or significant azimuthal flow in the neutral velocity distribution measurements. Measurements of the spatial dependence LIF intensity, neutral perpendicular temperature, and neutral radial flow (measured along the $y=0$ axis) are shown in Fig. 10. For helium and argon (discussed below) plasmas, the neutral temperatures are only slightly warmer than room temperature (~0.03 eV). The LIF intensity and neutral temperatures are largest near the axis of the discharge (peaks are displaced by −0.5 cm along the x axis). The radial component of the neutral flow is small, goes to zero at the location of the peak of the LIF signal, and is symmetric around the location of the zero flow velocity point.

An important feature of the helium neutral flow measurements is a recent reduction in the error bars on our LIF-based flow measurements. Our previous measurements of ion velocity distribution functions in helicon plasmas included an uncertainty on the order of 100 m/s. That value included statistical noise in the measurement as well as a systematic error that was not well understood. To obtain an absolute flow speed measurement, the shift in the peak of a measured vdf is compared to a simultaneously measured molecular iodine spectrum. Recently we learned of a systematic error in the published iodine spectral tables.[30] By correcting our values for the wavelengths of the large-amplitude features in the molecular iodine spectrum in the vicinity of the LIF absorption line and by lengthening the data acquisition interval compared to the lock-in integration time (so that $T_{\mathrm{sweep}}/T_{\mathrm{integration}} \sim 800$ for a single-pole low-pass filter) we have reduced the uncertainty in our flow measurements by a factor of 10. The low-pass filtering process of using lock-in amplification to extract the LIF signal from the emitted plasma light has significant effect on the shift of the measured line shape, even for $T_{\mathrm{sweep}}/T_{\mathrm{integration}} \sim 100$. Note that the LIF flow measurements shown in Figs. 3 and 4 were corrected for the approximately 150 m/s systematic flow error that we empirically determined arises in argon plasmas for $T_{\mathrm{sweep}}/T_{\mathrm{integration}}=300$ and our experimental apparatus. To the best of our knowledge, these high precision and high spatial resolution measurements are the first measurements of the radial neutral flow in a helicon source.

The LIF measurements presented thus far (along with Langmuir probe measurements of the plasma density profile), provide enough information for determination of the radial profile of the ion viscosity in an argon helicon plasma. However, determination of the radial profile of the ion-neutral momentum damping rate requires measurement of

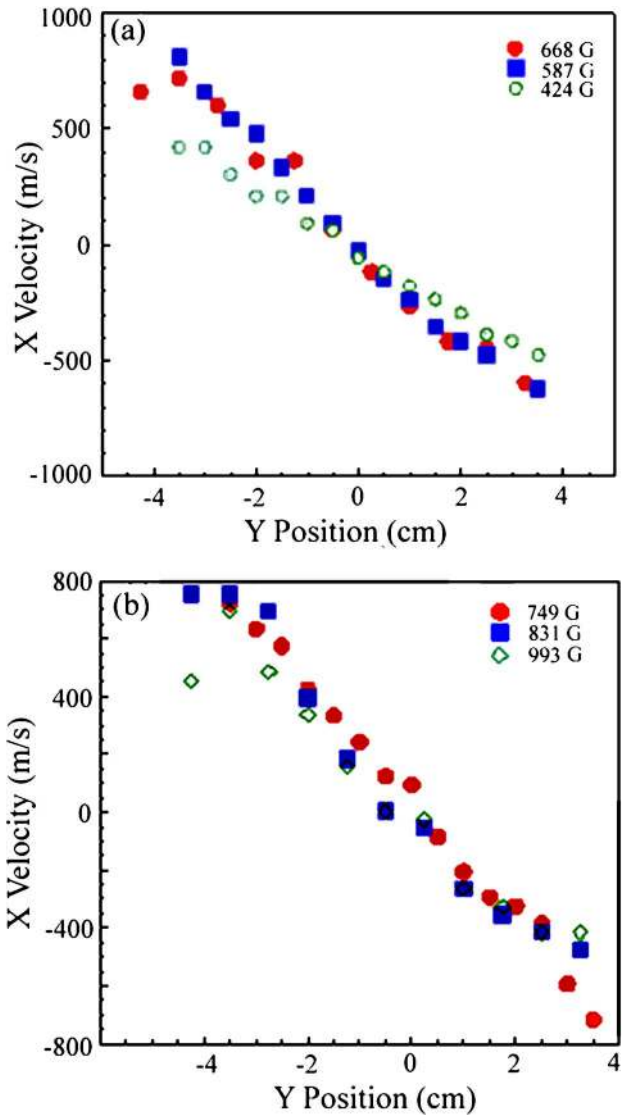

FIG. 7. (Color online) For a radio frequency of $f=9.5$ MHz, $P=6.7$ mTorr, $B_{\mathrm{LEIA}}=35$ G, and power=750 W, the horizontal ion flow velocity field vs y, i.e., radial, position for magnetic field strengths of (a) 424, 587, and 668 G, and (b) 749, 831, and 993 G.

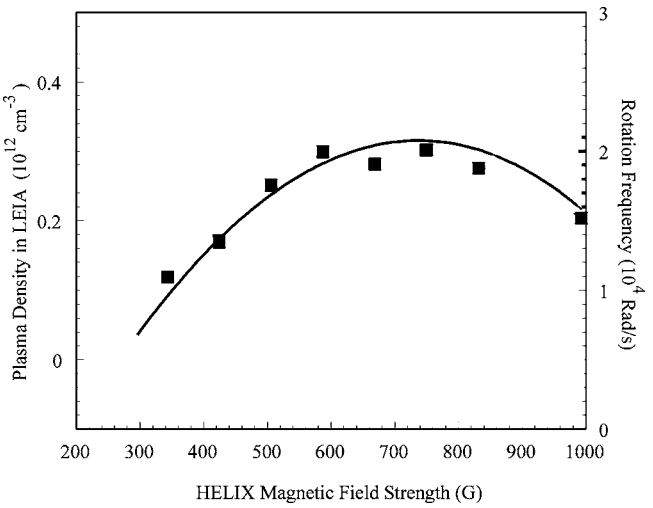

FIG. 8. For a radio frequency of $f=9.5$ MHz, $P=6.7$ mTorr, $B_{\mathrm{LEIA}}=35$ G, and power=750 W, the plasma rotation frequency (squares) and the plasma density in LEIA (solid line) vs magnetic field strength.

the ground state velocity distribution of argon neutrals. Because the LIF signal strength depends on population of a particular excited neutral state, the neutral density, electron temperature, and electron density profiles all contribute to the LIF intensity profile. Although Fig. 5 demonstrated that for high density, argon helicon plasmas the relationship between Ar II LIF intensity, plasma density, and electron temperature can be reduced to a relatively simple formula, no such simple formula is easily created for Ar I LIF. Simply put, measuring absolute neutral density as a function of position inside a high density plasma is much more difficult than measuring the plasma density.

To relate the ground state neutral density profile to the measured Ar I LIF intensity, electron temperature profile, and electron density profile, we employed a collisional radiative (CR) model originally developed by Vlček[31] and modified by Bogaerts *et al.*[32] that allows for the input of an arbitrary electron energy distribution function and includes interactions between the electron population and 65 energy levels of neutral argon.[31] The Bogaerts *et al.* modifications added details of the two 4*s* metastable levels of Ar I and fast argon ion and atom impact ionization and excitation.[32] CR model predictions of the Ar I excited state profiles based on the measured electron density and temperature profiles shown in Fig. 11 were compared to Abel inverted emission spectroscopy measurements and LIF measurements of the excited state profiles for a range of possible ground state neutral density profiles.[33,34] The measured neutral temperature profile and the model neutral profile that resulted in a CR model prediction that best fit the measured LIF intensity and emission profiles are shown in Figs. 12(a) and 12(b), respectively. The CR model and measured LIF and emission intensities are shown in Figs. 12(c) and 12(d), respectively. The LIF intensity profile is compared to the CR model predicted profile for the absorption, or lower, state density profile. Emission from the upper state of the Ar I LIF sequence was Abel inverted and compared to CR model predicted profile for the upper state of the Ar I LIF sequence.[33,34] The plasma density profile shown in Fig. 11(a) is similar in magnitude and shape to the plasma density profile reported in

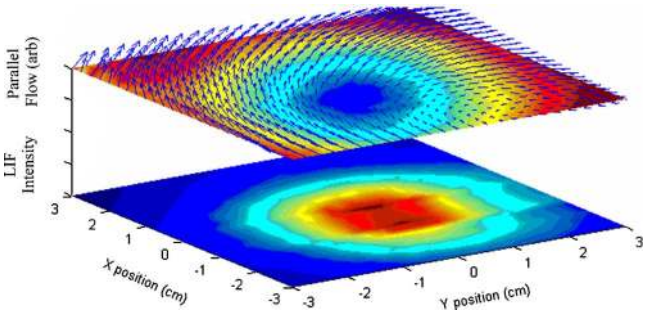

FIG. 9. (Color online) For a radio frequency of $f=9.5$ MHz, $P=3.8$ mTorr, $B_{\mathrm{HELIX}}=652$ G, $B_{\mathrm{LEIA}}=35$ G, and power=750 W, the full three-dimensional ion flow velocity across the plasma cross section (top) and the LIF signal amplitude (bottom). The magnitude of the z component of the ion velocity is overlaid as a color contour plot on the upper figure.

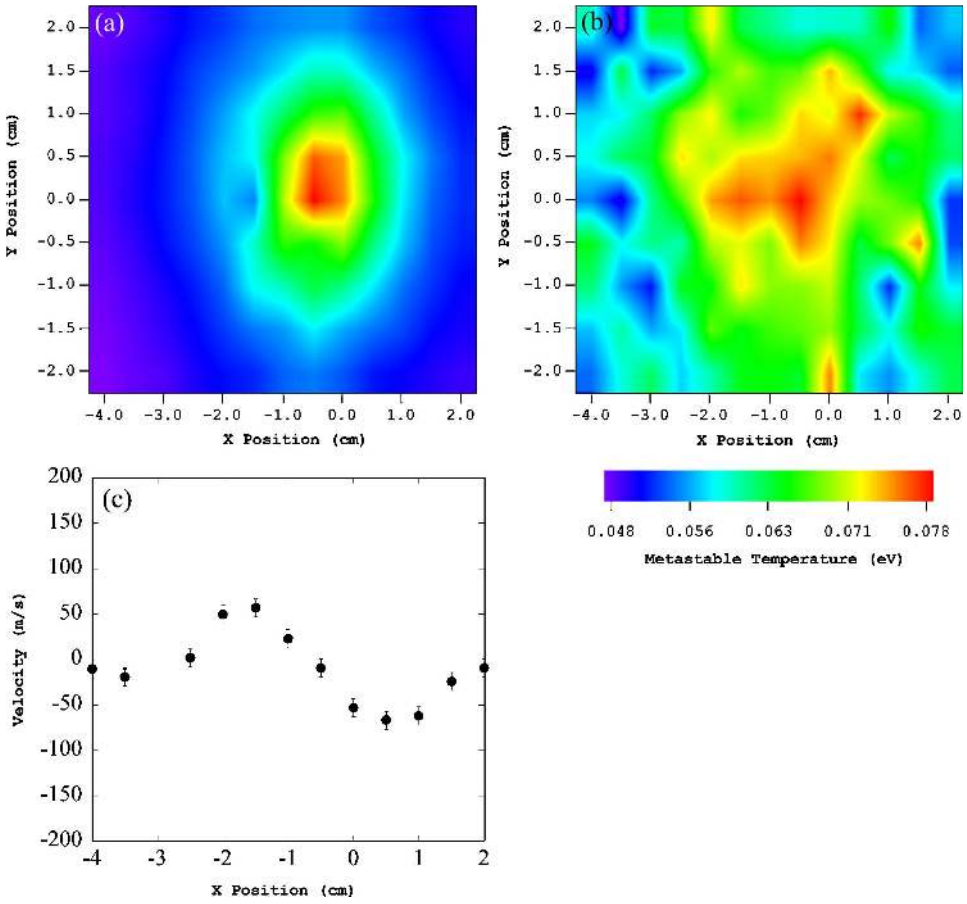

FIG. 10. (Color online) For a radio frequency of $f=9.5$ MHz, $P=34$ mTorr, $B_{\mathrm{HELIX}}=500$ G, $B_{\mathrm{LEIA}}=0$ G, and power=750 W, the helium neutral (a) LIF signal amplitude, (b) temperature, and (c) radial flow speed. Note that the plots are symmetric around $x\sim-0.5$ cm.

Holland *et al.*[1] However, as noted previously, the Ar I temperature shown in Fig. 12(a) is an order of magnitude smaller than assumed in the Holland *et al.*[1] work. The neutral temperature profile is slightly peaked on axis and ranges from 0.07 eV on axis to roughly 0.05 eV towards the edge of the discharge. The best fit neutral density profile [Fig. 12(b)] is smallest on axis; with a relative magnitude of 35% compared to the edge neutral density. The sharp boundary between the inner depletion region and a constant neutral density in the edge of the plasma is an artifact of the crudeness of the neutral density profile model function used in the CR model calculations.

IV. ION VISCOSITY AND ION-NEUTRAL COLLISION FREQUENCY PROFILES

In the Holland *et al.* work, the relationship between the Reynolds stress and the time-averaged azimuthal component of the ion momentum was given by

$$\frac{1}{r^2}\frac{\partial}{\partial r}(r^2\langle\tilde{V}_r\tilde{V}_\theta\rangle) = -\nu_{i-n}\langle V_\theta\rangle + \mu_{ii}\left(\frac{1}{r}\frac{\partial}{\partial r}(r\langle V_\theta\rangle) - \frac{\langle V_\theta\rangle}{r^2}\right), \tag{2}$$

where $\langle\tilde{V}_r\tilde{V}_\theta\rangle$ equaled the electrostatic turbulent Reynolds stress $\langle R\rangle=\langle\tilde{E}_r\tilde{E}_\theta\rangle/B_o^2$ under the assumption that the convecting velocity fluctuations were purely electrostatic, the ion viscosity was taken to be $\mu_{ii}=0.3\rho_i^2\nu_{ii}$, the ion-neutral momentum damping rate was taken to be $\nu_{i-n}=n_{\mathrm{gas}}V_{\mathrm{th}}(\sigma_{io}^{\mathrm{cx}}+\sigma_{io}^{\mathrm{elas}})$, ν_{ii} is the ion-ion collision frequency $[\nu_{ii}=4.8\times10^{-8}Z^4n_i\ln(\Lambda)/(T_i^{3/2}\sqrt{m_{\mathrm{ion}}/m_{\mathrm{proton}}})]$, ρ_i the ion gyroradius, and V_{th} the relative speed of ions to neutrals.

Based on the form of the ion viscosity given above and the measured profiles for ion temperature and plasma density, the ion viscosity versus normalized plasma radius for the HELIX helicon plasma source is shown in Fig. 13. Because the ion temperature is relatively flat, the ion viscosity profile is dominated by the plasma density profile. Also shown in Fig. 13 is the ion viscosity profile assumed by Holland *et al.* In general, their assumed profile underestimates the ion viscosity on axis and overestimates the fraction of the plasma column over which the ion viscosity is large. Since they found that "the magnitude of $\langle V_\theta\rangle$ was inversely proportional to μ_{ii} and had a somewhat complex dependence on the spatial profile of μ_{ii}," use of the measured profile shown in Fig. 13 would likely have a significant effect on the spatial profile of the flow predicted by their turbulence model.

For the inferred neutral density profile shown in Fig. 12, and the measured ion and neutral temperatures (the much smaller neutral temperature allows us to ignore the neutral velocity in calculating the center of mass velocity for ion-neutral collisions), the ion-neutral momentum transfer rate, $\nu_{i-n}=n_{\mathrm{gas}}V_{\mathrm{th}}(\sigma_{\mathrm{io}}^{\mathrm{cx}}+\sigma_{\mathrm{io}}^{\mathrm{elas}})$, profile is shown in Fig. 14. The kink in the collision rate curve around $(r/a)\sim0.4$ arises from the sharp, and unphysical, boundary in the model neutral density profile of Fig. 12(b). The important physics result of this

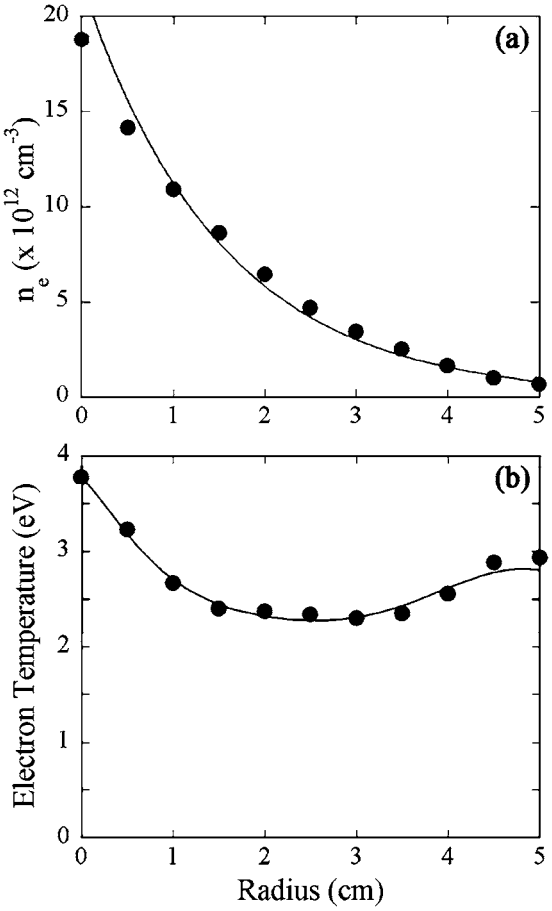

FIG. 11. (a) Electron density and (b) electron temperature obtained with rf-compensated Langmuir probe for magnetic field strength of 750 G, rf power of 300 W, pressure of 6.0 mTorr. Solid curves are the fits to the measurements used in the collisional radiative model.

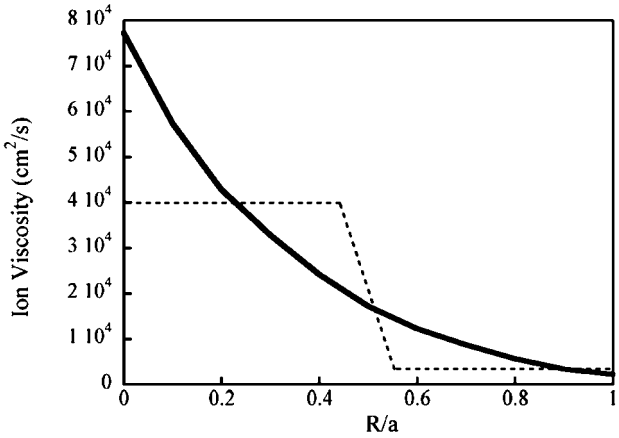

FIG. 13. Ion viscosity versus normalized radius (solid line) for a magnetic field strength of 750 G and a neutral pressure of 3.6 mTorr. Model function for ion viscosity (dashed line) used by Holland *et al.* (Ref. 1).

calculation is that the spatial dependence of the ion-neutral momentum rate closely tracks the neutral density profile, which increases towards the edge of a well-ionized helicon plasma. The similarity in spatial profiles occurs because the ion temperature profile is flat or slightly peaked at the edge of the discharge; the ion temperature is much larger than the neutral temperature; and the neutral density profile is hollow. The uniform value used in the Holland *et al.* study ($\sim 6 \times 10^3$ s^{-1}) differs significantly in both absolute magnitude and radial profile from the experimentally measured values.

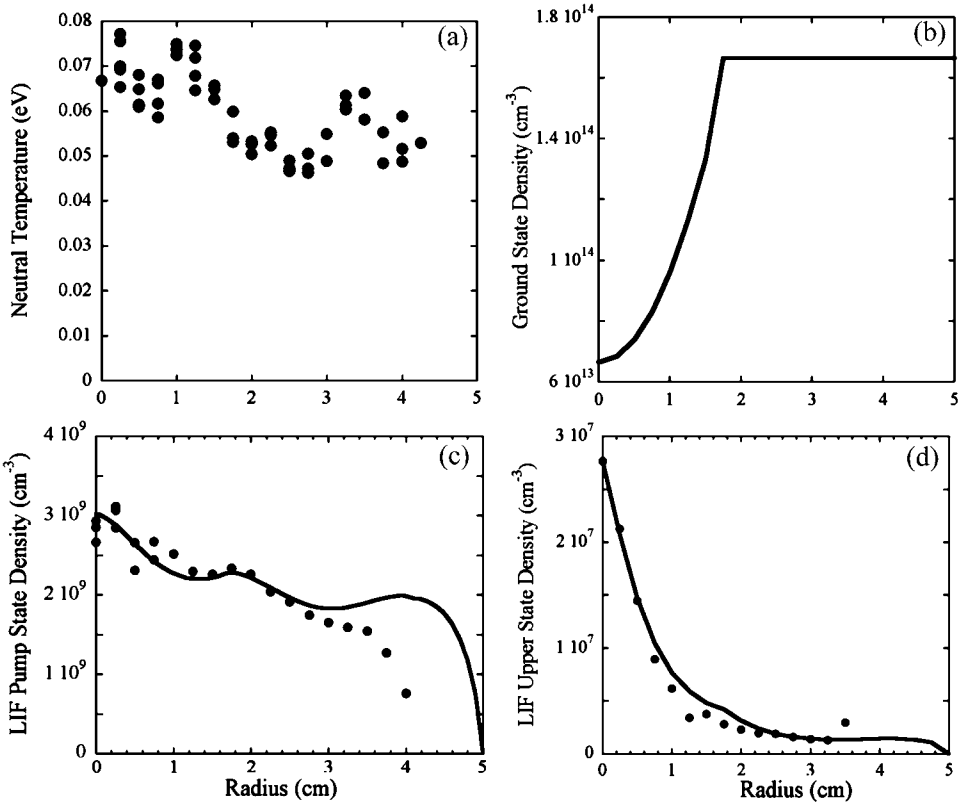

FIG. 12. (a) Neutral argon temperature, (b) best fit neutral density profile, and comparison of the collisional radiative model predicted excited state profiles (solid lines) to the (c) measured LIF intensity and (d) Abel inverted emission intensity from the upper state of the LIF sequence for magnetic field strength of 750 G, rf power of 300 W, pressure of 6.0 mTorr (Ref. 34).

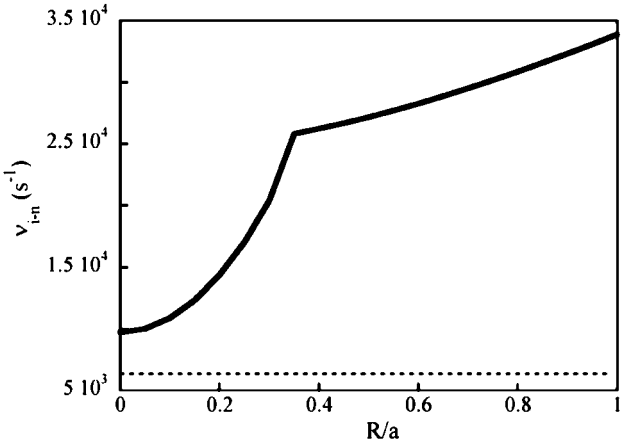

FIG. 14. Ion-neutral momentum transfer rate (solid line) for a magnetic field strength of 750 W and a neutral pressure of 3.6 mTorr. Assumed ion-neutral transfer rate (dashed line) used by Holland *et al.* (Ref. 1).

V. DISCUSSION

The measurements presented here demonstrate that azimuthal and parallel flows arise spontaneously in helicon sources with "open" ends. For large magnetic field strengths, substantial shear ($[1/\Omega_i]dV_\theta/dr \sim 0.2$) in the azimuthal flow also spontaneously develops near the edge of the plasma column. Such shear could lower the threshold for excitation for a variety of plasma instabilities. The LIF measurements indicate that for a wide range of plasma conditions, the argon ion temperature profile is essentially uniform across the helicon plasma column. Counter-intuitively, the parallel flow is largest at the edge of the HELIX source. Measurements of the equipotential contours at the end of an expanding current driven plasma at much lower pressure found that the equipotential contours associated with the spontaneously created internal double layer yielded the largest axial gradients in the potential at the edge of the discharge.[35] Similar phenomena in these experiments could be responsible for the increase in parallel flow at the edge of the helicon plasma.

LIF measurements of the radial flows of argon ions and helium neutrals indicates ions flow out radially at some hundreds of meters per second and there is a weak outward neutral flow,[23] perhaps fed by neutral gas flow along the axis of the device.

By combining the measured density and temperature profiles, it is possible to calculate the absolute magnitude of the ion viscosity and the ion-neutral momentum transfer rate as a function of position in the helicon source. The experimentally determined values are quite different than those recently used in theoretical models and therefore the model predictions should be re-examined in light of these new measurements.

[1] C. Holland, J. H. Yu, A. James, D. Nishijima, M. Shimada, N. Taheri, and G. R. Tynan, Phys. Rev. Lett. **96**, 195002 (2006).
[2] G. Ganguli, Y. C. Lee, and P. Palmadesso, Phys. Fluids **28**, 761 (1985); G. Ganguli, P. J. Palmadesso, and Y. C. Lee, Geophys. Res. Lett. **12**, (1985).
[3] M. E. Koepke, W. E. Amatucci, J. J. Carroll III, and T. E. Sheriden, Phys. Rev. Lett. **72**, 3355 (1994).
[4] E. Agrimson, N. D'Angelo, and R. L. Merlino, Phys. Rev. Lett. **86**, 5282 (2001).
[5] V. Gavrishchaka, M. Koepke, and G. Ganguli, Phys. Plasmas **3**, 3091 (1996).
[6] P. W. Terry, Rev. Mod. Phys. **72**, 109 (2000).
[7] A. M. Garofalo, Fusion Sci. Technol. **48**, 918 (2005).
[8] G. R. Tynan, M. J. Burin, C. Holland, G. Antar, N. Crocker, and P. H. Diamond, Phys. Plasmas **11**, 5195 (2004).
[9] J. L. Kline, E. Scime, R. Boivin, A. M. Keesee, X. Sun, and V. Mikhailenko, Phys. Rev. Lett. **88**, 1950 (2002).
[10] J. L. Kline, E. Scime, R. Boivin, A. M. Keesee, and X. Sun, Plasma Sources Sci. Technol. **11**, 413 (2002).
[11] E. E. Scime, P. A. Keiter, M. W. Zintl *et al.*, Plasma Sources Sci. Technol. **7**, 186 (1998).
[12] A. M. Keesee, R. Boivin, and E. Scime, Rev. Sci. Instrum. **75**, 4091 (2004).
[13] J. L. Kline, E. Scime, R. Boivin, A. M. Keesee, and X. Sun, Plasma Sources Sci. Technol. **11**, 413 (2002).
[14] R. A. Stern and J. A. Johnson III, Phys. Rev. Lett. **34**, 1548 (1975).
[15] D. N. Hill, S. Fornaca, and G. Wickman, Rev. Sci. Instrum. **54**, 309 (1983).
[16] R. McWilliams and D. Sheehan, Phys. Rev. Lett. **56**, 2485 (1986).
[17] D. A. Edrich, R. McWilliams, and N. S. Wolf, Rev. Sci. Instrum. **67**, 2812 (1996).
[18] X. Sun, C. Biloiu, R. Hardin, and E. Scime, Plasma Sources Sci. Technol. **13**, 359 (2004).
[19] R. Hardin, X. Sun, and E. Scime, Rev. Sci. Instrum. **75**, 4103 (2004).
[20] A. D. Bailey III, R. A. Stern, and P. M. Bellan, Phys. Rev. Lett. **71**, 3123 (1993).
[21] F. M. Levinton and F. Trintchouk, Rev. Sci. Instrum. **72**, 898 (2001).
[22] W. M. Ruyten and D. Keefer, AIAA J. **31**, 2083 (1993).
[23] C. Biloiu, X. Sun, E. Choueri, C. Compton, F. Doss, J. Heard, E. E. Scime, R. Specktor, and D. Ventura, Plasma Sources Sci. Technol. **14**, 766 (2005).
[24] L. Pauling and S. Goudsmit, *The Structure of Line Spectra* (McGraw-Hill, New York, 1930), p. 256.
[25] M. J. Goeckner, J. Goree, and T. E. Sheridan, Rev. Sci. Instrum. **64**, 996 (1993).
[26] H. R. Griem, *Principles of Plasma Spectroscopy* (Cambridge University Press, Cambridge, 1997), p. 160.
[27] R. W. P. McWhirter, *Spectral Intensities, in Plasma Diagnostics Techniques* (Academic, New York, 1965), p. 201.
[28] M. Light, F. F. Chen, and P. L. Colestock, Phys. Plasmas **8**, 4675 (2001).
[29] X. Sun, "A Study of Ion Acceleration, Asymmetric Optical Pumping and Low Frequency Waves in Two Expanding Helicon Plasmas," Ph.D. dissertation, West Virginia University, Morgantown, 2005.
[30] S. Gerstenkorn and P. Luc, J. Phys. (France) **46**, 867 (1985).
[31] J. Vlček, J. Phys. D **22**, 623 (1989).
[32] A. Bogaerts, R. Gijbels, and J. Vlcek, J. Appl. Phys. **84**, 121 (1998).
[33] A. Keesee and E. Scime, Rev. Sci. Instrum. **77**, 10F304 (2006).
[34] A. Keesee, "Neutral Density Profiles in Argon Helicon Plasmas," Ph.D. dissertation, West Virginia University, Morgantown, 2006.
[35] G. Hairapetian and R. L. Stenzel, Phys. Fluids B **3**, 899 (1991).